Металлофиз. новейшие технол. / Metallofiz. Noveishie Tekhnol.
2015, т. 37, № 5, сс. 581–591
Оттиски доступны непосредственно от издателя
Фотокопирование разрешено только
в соответствии с лицензией

ЭЛЕКТРОННЫЕ СТРУКТУРА И СВОЙСТВА

PACS numbers: 63.20.dk, 63.20.kd, 71.15.Mb, 71.15.Rf, 71.18.+y, 71.20.Ps, 74.70.Ad

Complex Investigation of the Fermi Surface in HfB_2

S. M. Sichkar and V. N. Antonov

G. V. Kurdyumov Institute for Metal Physics, N.A.S. of Ukraine,
36 Academician Vernadsky Blvd.,
UA-03680 Kyiv, Ukraine

The electronic structure, Fermi surface, angle dependence of the cyclotron masses, and extremal cross sections of the Fermi surface of the hafnium diboride are investigated from the first principles using the fully relativistic and full-potential linear muffin-tin orbitals' methods. A good agreement with experimental data of cyclotron masses and extremal cross sections of the Fermi surface is achieved.

Електронну структуру, поверхню Фермі, кутову залежність циклотронних мас і екстремальні перетини поверхні Фермі дибориду гафнію було досліджено з перших принципів із використанням повністю релятивістського та повнопотенціяльного методів лінійних МТ-орбіталей. Було досягнуто задовільного збігу з експериментальними даними стосовно циклотронних мас і екстремальних перетинів поверхні Фермі.

Электронная структура, поверхность Ферми, угловая зависимость циклотронных масс и экстремальные сечения поверхности Ферми диборида гафния были исследованы из первых принципов с использованием полностью релятивистского и полнопотенциального методов линейных МТ-орбиталей. Было достигнуто хорошее согласие с экспериментальными данными циклотронных масс и экстремальных сечений поверхности Ферми.

Key words: electronic structure, Fermi surface, cyclotron masses, LMTO, diborides.

(Received March 12, 2015)

1. INTRODUCTION

Ceramics based on transition-metal borides, nitrides and carbides have extremely high melting points (> 2500°C) and are referred to as ultra-

high temperature ceramics [1, 2]. Among them, diborides such as ZrB_2 and HfB_2 have a unique combination of mechanical and physical properties: high melting points (>3000°C); high thermal and electrical conductivity; chemical inertness against molten metals; great thermal shock resistance [1–3]. Thus, although carbides typically have the highest melting points (> 3500°C); the diborides ZrB_2 and HfB_2 are more attractive candidates for high-temperature thermomechanical structural applications at temperatures ≥ 3000°C [1, 2].

Potential applications include thermal protective structures for leading-edge parts on hypersonic re-entry space vehicles [1, 4], propulsion systems [1, 4], furnace elements [5], refractory crucibles [5], and plasma-arc electrodes [5, 6].

The discovery of superconductivity in MgB_2 at 39 K by Akimitsu [7] has led to booming activity in the physics community and activated a search for superconductivity in other diborides. Natural candidates for this search are MB_2-type light metal diborides (M = Li, Be, Al). However, up to now, superconductivity has not been reported in the majority of these compounds [8]. Only very recently superconductivity below 1 K ($T_c = 0.72$ K) has been reported in $BeB_{2.75}$ [9]. On the other hand, there is contradictory report about superconductivity up to $T_c = 9.5$ K in TaB_2 [10], which encourages further studies of these diborides.

By now, the de Haas–van Alphen (dHvA) measurements of the Fermi surface [11], optical ellipsometry measurements [12], magnetic susceptibility [13, 14], and NMR measurements [15], as well as first-principles calculations of the electronic structure of diborides including HfB_2 have been presented [13, 14, 16–19].

Vajeeston *et al.* [16] investigated the electronic structure of HfB_2 using the tight-bonding linear muffin-tin orbitals' method, they claimed that metal–metal and metal–boron interactions are less significant than the p–p covalent interaction of boron atoms.

Zhang *et al.* [17, 18] investigated theoretically the pressure dependence of elastic constants, bulk modulus and elastic anisotropy of HfB_2. The pressure dependence of structural property shows that the effect of pressure is little on the structure of HfB_2.

They found that high pressure greatly changes the profile of the density of states (DOS), but it hardly changes the DOS value at Fermi level. Meanwhile, the Mulliken population analyses are investigated. It was suggested that as the pressure increases, a number of charge transfer from Hf to B atoms takes place. Through quasi-harmonic Debye model, the variations of the Debye temperature, heat capacity, and thermal expansion with pressure and temperature were obtained and discussed.

Fedorchenko and Grechnev with co-authors [13, 14] measured the temperature dependences of the magnetic susceptibility χ and its ani-

sotropy $\Delta\chi = \chi_{\parallel} - \chi_{\perp}$ for single crystals of transition-metal diborides MB_2 (M = Sc, Ti, V, Zr, Hf) in the temperature interval 4.2–300 K. A transition into the superconducting state was not found in any of the diborides studied, right down to liquid-helium temperature. It was found that the anisotropy is weakly temperature-dependent, nonmonotonic function of the filling of the hybridized p–d conduction band. First-principles calculations of the electronic structure of diborides and the values of the paramagnetic contributions spin and Van Vleck to their susceptibility show that the behaviour of the magnetic anisotropy is caused by the competition between Van Vleck paramagnetism and orbital diamagnetism of the conduction electrons.

Li *et al.* [19] studied the thermodynamics of the oxidation of HfB_2 at temperatures of 1000, 1500, 2000, and 2500 K using volatility diagrams. They found that HfB_2 exhibits oxidation behaviour similar to ZrB_2.

The properties of the Fermi surface of ScB_2, ZrB_2, and HfB_2 single crystals were studied by Pluzhnikov *et al.* [11] using the de Haas–van Alphen effect. The angular dependences of the frequencies of the dHvA oscillations in the planes $(10\bar{1}0)$, $(11\bar{2}0)$ and (0001), and the values of their effective cyclotron masses were measured. The frequencies of the oscillations lie in the interval $(0.96–0.87)\cdot 10^2 T$ and the measured cyclotron masses m_c^* lie in the range $(0.09–0.87)m_0$.

Despite a lot of publications, there are still many open questions related to the electronic structure and physical properties of HfB_2 diboride. Up to now, there is no theoretical explanation of the real form of Fermi surface as well as angle dependence of the cyclotron masses and extremal cross sections of the Fermi surface in HfB_2.

The aim of this work is a complex investigation of the electronic structure, Fermi surface, angle dependence of the cyclotron masses, and extremal cross sections of the Fermi surface of the hafnium diboride. The paper is organized as follows. Section 2 presents the details of the lattice structure in HfB_2. Section 3 is devoted to the electronic structure. Section 4 focuses on angle dependence of the cyclotron masses and extremal cross sections of the Fermi surface. The results are compared with available experimental data. Finally, the main results are summarized in Sec. 5.

2. GEOMETRIC STRUCTURE OF HfB_2

It is simply a hexagonal lattice in which closely-packed transition-metal layers are present alternative with graphite-like B layers (Fig. 1). These diborides cannot be exactly layered compounds because the interlayer interaction is strong even though the M layers alternate with the B layers in their crystal structure. The boron atoms lie on the corners of hexagons with the three nearest neighbour boron atoms in

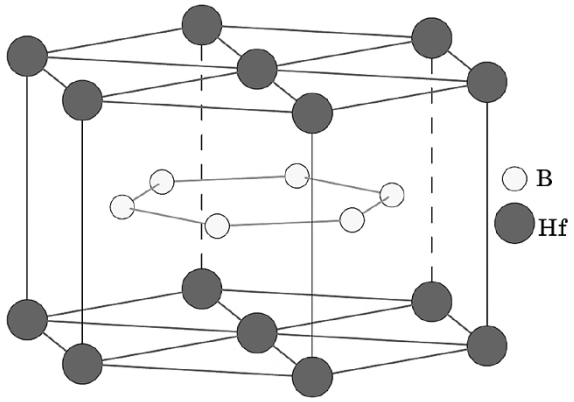

Fig. 1. Schematic representation of the HfB_2 crystal structure.

each plane. The M atoms lie directly in the centres of each boron hexagon, but midway between adjacent boron layers. Each transition metal atom has twelve nearest neighbour B atoms and eight nearest neighbour transition metal atoms (six are on the metal plane and two out of the metal plane). There is one formula unit per primitive cell and the crystal has simple hexagonal symmetry (D_{6h}).

3. ENERGY BAND STRUCTURE

Figure 2 presents the energy band structure and total density of states of HfB_2. The partial DOSs for HfB_2 are shown in Fig. 3. Our results for the electronic structure of HfB_2 are in agreement with earlier calculations [14, 16]. A common feature for all transition metal diborides is the deep DOS minimum (pseudo-gap) at the Fermi energy separating the valence band and the conduction band. According to Pasturel *et al.* [20], a pseudo-gap arises because of a strong chemical interaction. The M–B covalent bonding is believed to be responsible for this effect. The

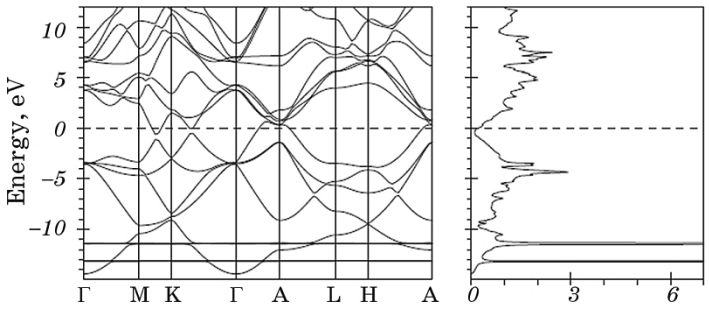

Fig. 2. Energy band structure and total DOS [in states/(cell eV)] of HfB_2.

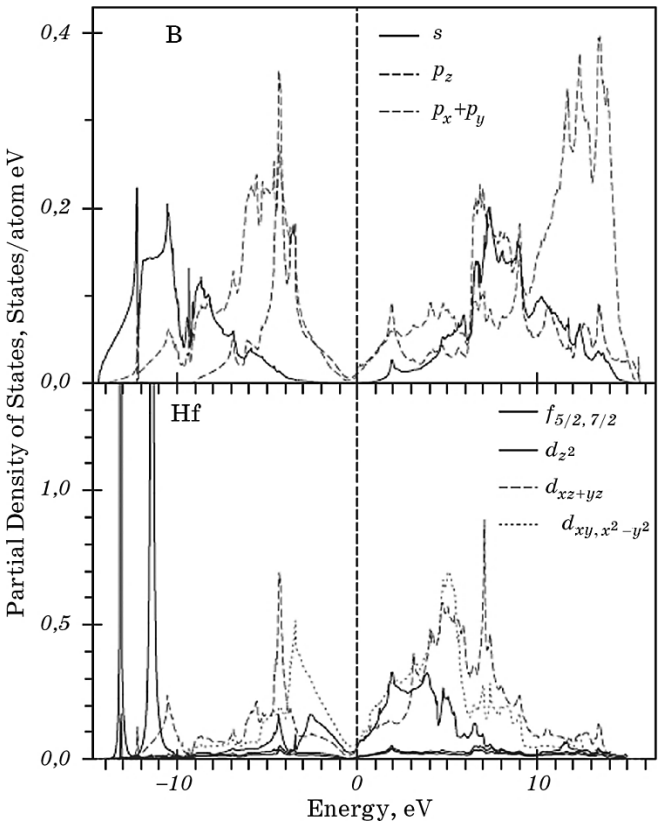

Fig. 3. Partial DOSs [in states/(atom eV)] of HfB_2.

Hf4$f_{5/2,7/2}$ states in HfB_2 are situated at the −14.5 eV to −10 eV. The Hf5d states are the dominant features in the interval from −12.5 eV to 14 eV. These tightly bound states show overlap with B2p and, to a lesser extent, with B2s states both above and below ε_F, implying considerable covalence. Higher-energy states between 9 eV and 17 eV above ε_F appear to arise from Hf6p and 6s states hybridized with B2p states.

The crystal field at the Hf site (D_{6h} point symmetry) causes the splitting of Hfd orbitals into a singlet a_{1g} (d_{3z^2-1}) and two doublets e_{1g} (d_{yz} and d_{xz}) and e_{2g} (d_{xy} and $d_{x^2-y^2}$). The crystal field at the B site (D_{3h} point symmetry) causes the splitting of Bp orbitals into a singlet a_4 (p_z) and a doublet e_2 (p_x and p_y). Bs states occupy a bottom of valence band between −14.6 eV and −3.0 eV and hybridize strongly with Bp_x and p_y and Hfd_{yz} and d_{xz} states located at −12.5 eV to −0.5 eV. Bp_x and p_y occupied states are located between −12.5 eV and −0.5 eV. Bp_z states occupied a smaller energy interval from −7.5 eV to −0.5 eV with a very strong and narrow peak structure at around −4 eV.

4. FERMI SURFACE

The Fermi surfaces (FS) of ScB_2, HfB_2, and HfB_2 were studied by Pluzhnikov *et al.* [11] using the dHvA effect. Theoretical calculations show a ring-like electron FS around the *K* symmetry point (Fig. 4) and of a wrinkled dumbbell-like hole FS at the *A* point (Fig. 5) in HfB_2. The electron and hole Fermi surfaces have threefold and sixfold symmetries, respectively.

Figure 6 shows the calculated cross section areas in the plane perpendicular *z* direction and crossed *A* symmetry point for hole FS (upper panel) and crossed Γ point for electron FS (lower panel) of HfB_2.

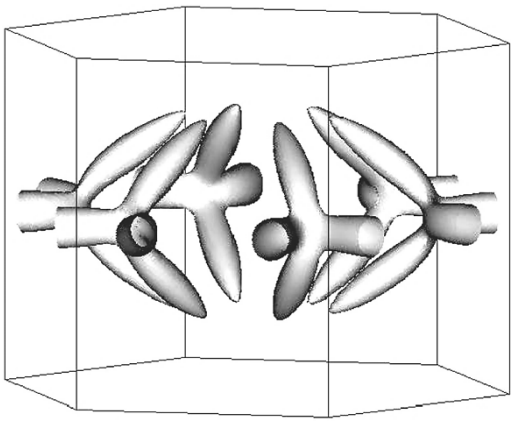

Fig. 4. The calculated electron sheets of the Fermi surface around *K* symmetry point from the 6th energy band of HfB_2.

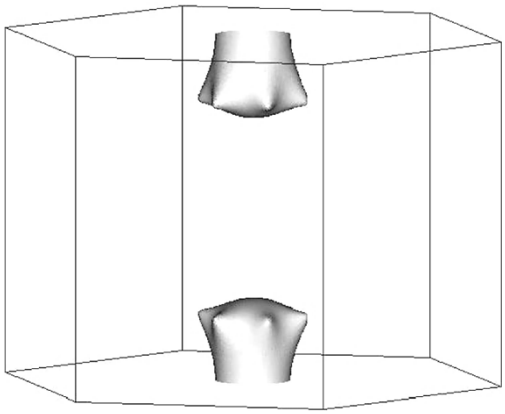

Fig. 5. The calculated hole sheets of the Fermi surface at the *A* symmetry point from the 5th energy band of HfB_2.

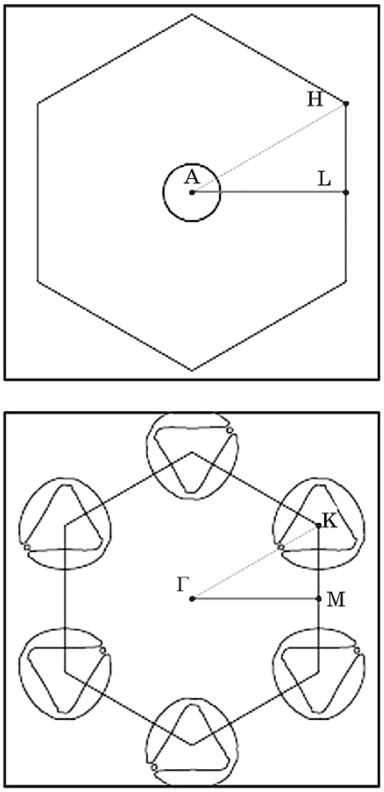

Fig. 6. The calculated cross-sections in the plane perpendicular *z* direction and crossed *A* symmetry point (upper panel) and Γ point (lower panel) for HfB_2 (full curves).

Figure 7 represents angular variations of the experimentally measured dHvA frequencies [11] for HfB_2 in comparison with the first-principle calculations for field direction in the $(10\bar{1}0)$, $(11\bar{2}0)$, and (0001) planes. The observed frequencies of α, β, γ, and δ oscillations belong to electron FS around the *K* point. The ε, μ, and ζ orbits belong to the hole wrinkled dumbbell FS. The α frequencies have four branches at the $(10\bar{1}0)$ plane and three branches at the $(11\bar{2}0)$ plane. The lower γ frequencies have one branch in both planes. The theory reasonably well reproduces the frequencies measured experimentally. However, there are still some discrepancies. The β orbits have additional two branches at higher frequencies on the $(11\bar{2}0)$ and (0001) planes not observed experimentally. The experiment for high frequencies detected only ε orbits in vicinity of the <0001> direction in HfB_2. We found ε, μ and ζ orbits similar to the corresponding orbits observed experimentally in isostructural and isovalent ZrB_2 [11].

These orbits have not been detected in the dHvA experiment [11].

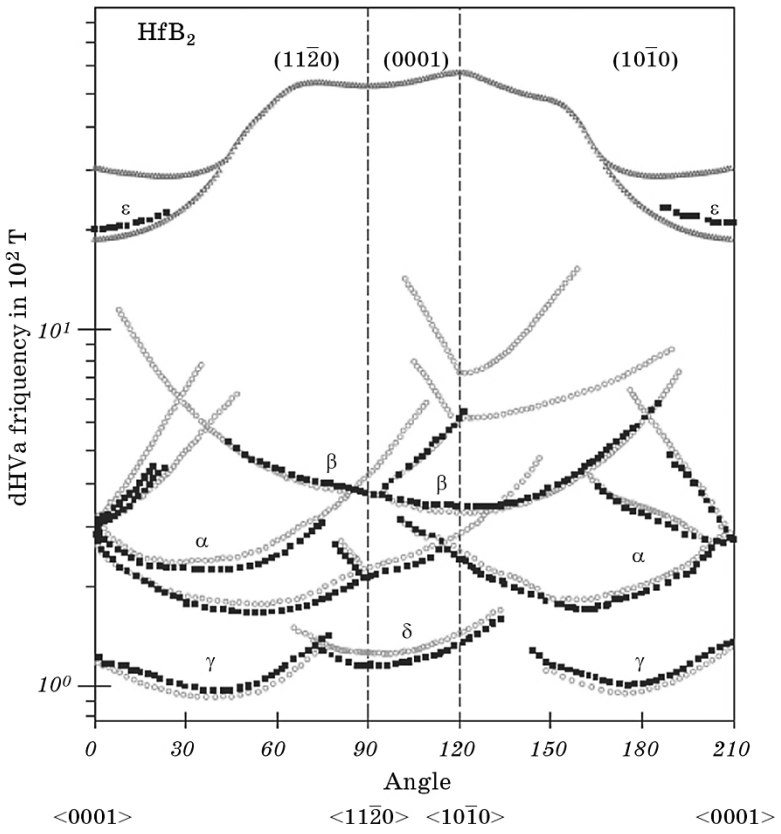

Fig. 7. The calculated (open circles for the electron (lower part) and hole (upper part) surfaces) and experimentally measured [11] (black full squares) angular dependence of the dHvA oscillation frequencies in the HfB_2 compound.

One of the possible reasons for that is the relatively large cyclotron mass for these orbits. Figure 8 shows the theoretically calculated angular dependence of the cyclotron masses (m_b) and the experimentally measured masses (m_c^*) for high-symmetry directions in HfB_2.

The cyclotron effective masses were determined from the temperature dependences of the amplitudes of the dHvA oscillations. The cyclotron masses for ε, μ, and ζ orbits in HfB_2 are much higher than the corresponding low-frequency oscillations α, β, γ, and δ.

The fact that the masses for electron Fermi surface are significantly larger than for the hole one may explain a negative experimentally measured Hall coefficient [21] and confirms electrons as the dominant charge carriers in HfB_2. A Wiedemann–Franz analysis also indicates the dominance of electronic contributions to heat transport [21].

We note that band cyclotron effective masses m_b are renormalized by the electron–phonon interaction $m_c^* = m_b(1 + \lambda)$, where λ is the constant

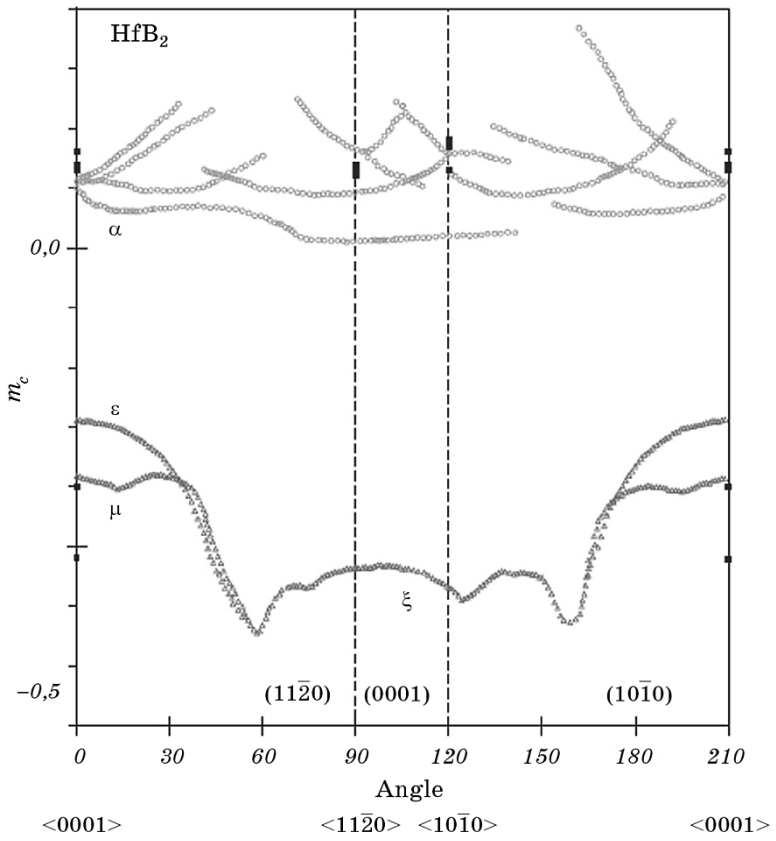

Fig. 8. The calculated angular dependence of the cyclotron masses for the electron Fermi surface (open circles in upper part) and the hole Fermi surface (open triangles in lower part) and experimentally measured ones [11] (black full squares) in the compound HfB_2.

of the electron–phonon interaction.

By comparing the experimentally measured cyclotron masses with band masses, we can estimate the λ. It is strongly varied on the orbit type and magnetic direction. We estimate the constant of the electron-phonon interaction to be equal to 0.18–0.23 for the α orbits and 0.36 and 0.75 for the ε and μ orbits respectively, with $H \parallel$ <0001>). For the <10$\bar{1}$0> and <11$\bar{2}$0> directions, the λ for the α orbits are reduced (to 0.10 and 0.12 values, respectively).

5. SUMMARY

We investigated in details the Fermi surface, angle dependence of the cyclotron masses, and extremal cross sections of the Fermi surface of

HfB_2. Theoretical calculations show a ring-like electron FS in HfB_2 around the K symmetry point and a wrinkled dumbbell-like hole FS at the A point. Theory reproduces the experimentally measured dHvA frequencies in HfB_2 reasonably well. We found that masses for low-frequency oscillations α, β, γ, and δ are less than $0.25m_0$. Masses for high-frequency oscillations ε, μ, and ζ lie in the range from -0.3 to $-0.65m_0$. The experiment for high frequencies detected only ε orbits in vicinity of the <0001> direction in HfB_2. We found ε, μ , and ζ orbits similar to the corresponding orbits observed experimentally in isostructural and isovalent ZrB_2 [11]. These orbits have not been detected in the dHvA experiment. One of the possible reasons for that is the relatively large cyclotron mass for these orbits.

REFERENCES

1. K. Upadhya, J. M. Yang, and W. P. Hoffmann, *Am. Ceram. Soc. Bull.*, **76**: 51 (1997).
2. W. G. Fahrenholtz, G. E. Hilmas, I. G. Talmy, and J. A. Zaykoski, *J. American Ceramic Society*, **90**: 1347 (2007).
3. C. Mroz, *Am. Ceram. Soc. Bull.*, **73**: 141 (1994).
4. A. S. Brown, *Aerospace Am.*, **35**: 20 (1997).
5. K. Kuwabara, *Bull. Ceram. Soc. Jpn.*, **37**: 267 (2002).
6. S. Norasetthekul, P. T. Eubank, W. L. Bradley, B. Bozkurt, and B. Stucker, *J. Mater. Sci.*, **34**: 1261(1999).
7. J. Nagamatsu, N. Nakagawa, T. Muranaka, Y. Zenitani, and J. Akimitsu, *Nature (London)*, **410**: 63 (2001).
8. V. A. Gasparov, N. S. Sidorov, I. I. Zverkova, and M. P. Kulakov, *JETP Lett.*, **73**: 532 (2001).
9. D. P. Young, P. W. Adams, J. Y. Chan, and F. R. Fronczek, *Preprint Cond-Mat/0104063* (2001).
10. C. Buzea and T. Yamashita, *Supercond. Sci. Technol.*, **14**: R115 (2001).
11. V. B. Pluzhnikov, I. V. Svechkarev, A. V. Dukhnenko, A. V. Levchenko, V. B. Filippov, and A. Chopnik, *Low Temp. Phys.*, **33**: 350 (2007).
12. Y. Yang, S. Jayaraman, B. Sperling, D. Y. Kim, G. S. Girolami, and J. R. Abelson, *J. Vacuum Sci. Technol. A*, **25**: 200 (2007).
13. G. E. Grechnev, A. V. Fedorchenko, A. V. Logosha, A. S. Panfilov, I. V. Svechkarev, V. B. Filippov, A. B. Lyashchenko, and A. V. Evdokimova, *J. Appl. Cryst.*, **481**: 75 (2009).
14. A. V. Fedorchenko, G. E. Grechnev, A. S. Panfilov, A. V. Logosha, I. V. Svechkarev, V. B. Filippov, A. B. Lyashchenko, and A. V. Evdokimova, *Low Temp. Phys.*, **35**: 82 (2009).
15. C. S. Lue and W. J. Lai, *phys. status solidi (b)*, **242**: 1108 (2005).
16. P. Vajeeston, P. Ravindran, C. Ravi, and R. Asokamani, *Phys. Rev. B*, **63**: 045115 (2001).
17. J. D. Zhang and X. L. Cheng, *Physica B*, **405**: 3532 (2010).
18. J. D. Zhang, X. L. Cheng, and D. H. Li, *J. Alloys Compd.*, **509**: 9577 (2011).
19. H. Li, L. Zhang, Q. Zeng, and L. Cheng, *J. Phase Equilib. Diffus.*, **32**: 422

(2011).
20. A. Pasturel, C. Colinet, and P. Hichter, *Physica B*, **132**: 177 (1985).
21. L. Zhang, D. A. Pejakovic, J. Marschall, and M. Gasch, *J. American Ceramic Society*, **94**: 2562 (2011).